RSC Advances

PAPER

View Article Online
View Journal | View Issue

Cite this: *RSC Adv.*, 2025, **15**, 40006

Novel B,N-doped carbon quantum dot fluorescence quenching method for sensitive and green determination of lisinopril: mechanistic insights from quantum calculations and sustainable analytical approach

Taha Alqahtani,[a] Ali Alqahtani,[a] Adil Alshehri[b] and Ahmed A. Almrasy *[c]

A novel, sensitive, and environmentally friendly fluorescence quenching method was developed for lisinopril determination using boron and nitrogen co-doped carbon quantum dots (B,N CQDs) as fluorescent probes. The B,N CQDs exhibited uniform nanoparticles with mean diameter of 3.97 nm and intense blue fluorescence with maximum excitation at 360 nm and emission at 429 nm. Upon increasing lisinopril concentration, a quenching of the B,N CQDs fluorescence was observed in a concentration-dependent manner. The fluorescence quenching mechanism was investigated through Stern–Volmer analysis, thermodynamic studies, and quantum mechanical calculations. Static quenching *via* ground-state complex formation was confirmed with Stern–Volmer constants (K_{sv}) decreasing from 7.94×10^5 to 5.48×10^5 M^{-1} as temperature increased from 298 to 313 K. Quantum mechanical studies using the PM6 method revealed binding energy of −33.58 kJ mol^{-1}, in excellent agreement with experimental thermodynamic parameters ($\Delta G = -35.01$ kJ mol^{-1}). Two distinct interaction sites were identified: amino group of lisinopril with carboxylic group of B,N CQDs (4.4 Å) and carboxylic group of lisinopril with boron atom (3.6 Å). Experimental conditions were optimized using Box–Behnken response surface methodology. The developed method demonstrated a linear range of 0.02–2.0 μg mL^{-1}, detection limit of 6.21 ng mL^{-1}, and quantification limit of 18.63 ng mL^{-1}. Method validation according to ICH Q2(R2) guidelines confirmed satisfactory accuracy (98.14 ± 0.857%) and precision (RSD < 1.25%). The method was successfully applied to commercial tablets and spiked plasma samples with excellent recovery (97.46–103.64%). Comprehensive greenness assessment using Analytical GREEnness Metric (AGREE), Modified Green Analytical Procedure Index (MoGAPI), Blue Applicability Grade Index (BAGI), and Click Analytical Chemistry Index (CACI) yielded scores of 0.77, 80%, 77.5, and 70, respectively. This work represents the first report of B,N CQDs for lisinopril determination, offering cost-effectiveness, room-temperature operation, and superior environmental profile.

Received 17th July 2025
Accepted 15th October 2025

DOI: 10.1039/d5ra05164a

rsc.li/rsc-advances

1. Introduction

Angiotensin-converting enzyme (ACE) inhibitors represent one of the most widely prescribed therapeutic classes in cardiovascular medicine, serving as cornerstone treatments for hypertension, heart failure, chronic kidney disease, and post-myocardial infarction management.[1,2] Among the ACE inhibitor family, lisinopril has emerged as a particularly significant therapeutic agent, prescribed for nearly three decades to manage hypertension and reduce cardiovascular strain through competitive inhibition of the angiotensin-converting enzyme.[3] The clinical importance of lisinopril extends beyond blood pressure management, as it demonstrates proven efficacy in preventing major cardiovascular events, including acute myocardial infarction, stroke, and heart failure hospitalization, while providing renoprotective effects in diabetic nephropathy.[4] As a non-prodrug ACE inhibitor with predominantly renal elimination and favorable pharmacokinetic properties, lisinopril remains one of the most commonly prescribed ACE inhibitors worldwide, reflecting its widespread clinical acceptance and therapeutic utility.[5,6] The extensive clinical application of lisinopril necessitates robust therapeutic drug monitoring and stringent quality control protocols to ensure optimal therapeutic outcomes, particularly given the critical importance of dose optimization and the potential for serious adverse effects

[a]*Department of Pharmacology, College of Pharmacy, King Khalid University, Abha, 62529, Saudi Arabia*
[b]*Department of Medicine, College of Medicine, King Khalid University, Abha, 62529, Saudi Arabia*
[c]*Pharmaceutical Analytical Chemistry Department, Faculty of Pharmacy, Al-Azhar University, Cairo, 11751, Egypt. E-mail: ahmedalialmrasy8@gmail.com*

including hyperkalemia, acute kidney injury, and angioedema.[7] Furthermore, the pharmaceutical industry's commitment to quality assurance requires sophisticated analytical methodologies for lisinopril quantification in both bulk drug substances and pharmaceutical formulations, supporting regulatory compliance with International Council for Harmonisation (ICH) guidelines and ensuring consistent therapeutic efficacy across diverse patient populations.[8]

Current analytical methods for lisinopril determination include various techniques, but each has their advantages and limitations that could restrict routine use. HPLC methods have been widely developed for pharmaceutical analysis of lisinopril.[9–11] For example Beasley *et al.* established a stability-indicating HPLC method with high sensitivity (LOD 0.0075 μg mL^{-1}), but the method requires lengthy gradient elution times and complex mobile phase optimization that reduces analytical throughput.[9] LC-MS/MS approaches offer superior sensitivity for bioanalytical applications such as the work presented by Shah *et al.* which achieved high performance with LOQ of 0.50 ng mL^{-1} in human plasma using triple quadrupole MS, but the method requires expensive instrumentation, complex solid phase extraction using Waters Oasis HLB cartridges, and specialized technical expertise that limits laboratory accessibility.[12] Another method by Qin *et al.* was developed using LC-MS/MS with LOQ of 1.03 ng mL^{-1}, yet demands sophisticated mass spectrometric detection and high operational costs.[13] Interestingly, electrochemical methods provide cost-effective alternatives but face selectivity challenges. For example, Coldibeli *et al.* developed voltammetric methods using boron-doped diamond electrodes with detection limits of 3.05 nmol L^{-1}, but these methods suffer from electrode fouling and require specialized electrode materials.[14] Spectrofluorimetric methods have gained attention for lisinopril determination due to their sensitivity, but face significant practical limitations. El-Emam *et al.* (2004) achieved high sensitivity using NBD-Cl derivatization with LOD of 0.008 μg mL^{-1} through HPLC-fluorescence detection, but requires expensive NBD-Cl reagent, elevated temperature (60 °C), and extended reaction time (70 minutes) that reduces analytical throughput.[15] A recent method by Mohammed *et al.* introduced fluorescamine as a room-temperature probe achieving LOD of 0.182 μg mL^{-1}, but still requires expensive fluorescamine reagent and alkaline pH conditions.[16] However, these fluorimetric methods suffer from several drawbacks. The derivatization procedures are time-consuming and require expensive reagents. Moreover, the methods are susceptible to interference from endogenous amino acids in biological samples. These limitations restrict their routine application and highlight the need for simpler, more cost-effective fluorescence-based approaches.

Carbon quantum dots (CQDs) have emerged as promising fluorescent nanomaterials for analytical chemistry applications, representing a paradigm shift from traditional semiconductor quantum dots toward more sustainable and biocompatible alternatives.[17] Since their discovery during carbon nanotube purification in 2004, CQDs have demonstrated remarkable analytical potential due to their unique size-dependent optical properties, excellent water solubility, low toxicity, and cost-effective synthesis from renewable precursors.[18,19] The incorporation of heteroatoms, particularly boron and nitrogen co-doping, has significantly enhanced the optical and analytical performance of CQDs through synergistic electronic structure modifications that create new energy levels and narrow the HOMO–LUMO gap.[20,21] B,N-doped CQDs exhibit superior quantum yields ranging from 15–59%, representing up to 12-fold improvements over undoped systems, while maintaining excellent photostability and pH tolerance across physiological ranges.[22] These enhanced properties have enabled remarkable achievements in pharmaceutical analysis, with recent studies demonstrating nanomolar detection limits for various drug molecules including tetracycline (1 nM), dopamine (11 nM), and phenolic compounds (0.024–0.05 μM) through different fluorescence quenching mechanisms.[23–25] These mechanisms primarily involve static quenching, photoinduced electron transfer, and inner filter effects, providing high selectivity and sensitivity for pharmaceutical compounds containing amino groups and aromatic systems.[26] Despite these advances, the application of B,N-doped CQDs for ACE inhibitor determination remains largely unexplored, particularly for lisinopril, which presents unique analytical challenges due to its lack of strong chromophores and the complexity of biological matrices. Furthermore, as discussed earlier current fluorescence-based methods for lisinopril analysis suffer from expensive derivatization reagents and elevated temperature requirements highlighting the need for more practical and cost-effective analytical approaches.

Therefore, this study aims to develop and validate a novel, sensitive, and environmentally friendly "turn-off" fluorescence quenching method for lisinopril determination using boron and nitrogen co-doped carbon quantum dots (B,N CQDs) as fluorescent probes. The specific research objectives are: (1) to synthesize and comprehensively characterize B,N CQDs through physicochemical and optical techniques including size distribution, surface morphology, and structural analysis; (2) to investigate the fluorescence quenching mechanism between B,N CQDs and lisinopril using Stern–Volmer kinetics, thermodynamic studies, and quantum mechanical calculations to understand molecular-level interactions; (3) to systematically optimize experimental conditions (pH, B,N CQDs concentration, and reaction time) through Box–Behnken response surface methodology; (4) to validate the developed method according to ICH guidelines evaluating linearity, precision, accuracy, robustness, selectivity, and detection limits; (5) to demonstrate practical applicability through analysis of real pharmaceutical formulations and biological samples; and (6) to conduct comprehensive environmental assessment using different green analytical chemistry metrics to establish the method's sustainability profile. This work represents a novel report of B,N CQDs for lisinopril determination, offering advantages including cost-effectiveness, room-temperature operation, and superior environmental profile compared to conventional methods.

2. Experimental

2.1. Materials and reagents

Lisinopril reference standard (99.70% purity) was acquired from the Egyptian Drug Authority (EDA), Cairo, Egypt. High-

purity reagents for B,N CQDs synthesis including citric acid monohydrate, boric acid, and urea were obtained from El-Nasr Pharmaceutical Chemicals Co (Cairo, Egypt). HPLC-grade acetonitrile and orthophosphoric acid were sourced from Merck (Darmstadt, Germany). Other analytical-grade chemicals including sodium hydroxide, hydrochloric acid, and glacial acetic acid were also purchased from El-Nasr Pharmaceutical Chemicals Co (Cairo, Egypt). Commercial lisinopril tablets (Zestril®, 10 mg per tablet) were obtained from local pharmacies in Cairo, Egypt. Distilled water was utilized throughout all experimental procedures. Human plasma samples were procured from VACSERA CO., Giza, Egypt, and maintained at −20 °C prior to analysis.

Britton–Robinson universal buffer systems were freshly prepared for each analytical session by combining equimolar amounts (0.04 M each) of orthophosphoric acid, boric acid, and glacial acetic acid. pH adjustment was achieved using standardized 0.2 M sodium hydroxide solution. All buffer pH values were confirmed using a calibrated pH meter to maintain accuracy within ±0.05 pH units.

2.2. Instrumentation

Fluorescence spectroscopic measurements were performed using a Jasco FP-6200 spectrofluorometer featuring a 150 W xenon light source. Operating parameters were set as follows: excitation and emission bandwidths of 10 nm, scanning velocity of 4000 nm min^{-1}, and emission detection range of 375–600 nm. Measurements were conducted in 1 cm optical path length quartz cells with four-sided polished surfaces for maximum transmission efficiency. UV-visible spectrophotometric analysis was carried out using a Shimadzu UV-1800 instrument with 1 cm quartz cells over the wavelength range of 200–800 nm. pH determinations were made using a Jenway 3505 pH meter fitted with a combination glass electrode (accuracy ±0.01 pH units). Electrode calibration was performed using certified buffer standards (pH 4.01, 7.00, and 10.01) before each measurement series.

Particle size analysis was conducted using dynamic light scattering (DLS) on a Malvern Zetasizer Nano ZS system. Morphological characterization was performed *via* transmission electron microscopy (TEM) using a JEOL JEM-2100 instrument operated at 200 kV. Structural analysis was accomplished through Fourier-transform infrared (FTIR) spectroscopy using a Nicolet iS5 FT-IR spectrometer across the wavenumber range of 4000–400 cm^{-1} with 4 cm^{-1} resolution. Samples were prepared as KBr pellets using the standard pelletization technique. Elemental composition of the purified B,N-CQDs was determined using CHN elemental analysis (PerkinElmer 2400 Series II CHNS/O analyzer).

2.3. Synthesis and characterization of B,N CQDs

B,N CQDs were synthesized using a thermal decomposition method adapted from previous reports[27] with modifications for enhanced analytical performance. Citric acid (0.5 g) and boric acid (0.1 g) were completely dissolved in 50 mL of deionized water under magnetic stirring. Urea (0.2 g) was subsequently added as the nitrogen source, and the mixture was stirred vigorously for 30 minutes to ensure complete dissolution and homogenization. The precursor solution was transferred to a teflon-lined stainless-steel autoclave and placed in a muffle furnace preheated to 200 °C. The thermal treatment was maintained for 3 hours under ambient atmosphere conditions to facilitate carbonization and heteroatom doping processes. During heating, the initially colorless solution gradually transformed to yellow, then orange, and finally to dark brown, indicating successful carbon framework formation and heteroatom incorporation. After cooling to room temperature, the product was dissolved in 20 mL of deionized water and sonicated for 15 minutes to ensure complete dissolution. The resulting brown solution was filtered through a 0.22 μm membrane filter to remove any undissolved particles or large aggregates. Purification was achieved through dialysis using a cellulose membrane (molecular weight cut-off 1000 Da) against deionized water for 48 hours with water changes every 8 hours to remove unreacted precursors and low molecular weight impurities. After dialysis, the purified solution was evaporated to dryness using rotary evaporation at 40 °C under reduced pressure to obtain the final purified B,N CQDs as a solid product with a yield of 134.2 mg (16.78% based on 800 mg total starting materials). The purified solid was redispersed in deionized water to prepare a stock solution with concentration of 1.0 mg mL^{-1}. The stock solution was stored at 4 °C in amber glass vials and showed stable fluorescence properties for at least 10 days. Comprehensive characterization of the synthesized B,N CQDs included morphological analysis by TEM, size distribution by DLS, optical properties evaluation through UV-vis and fluorescence spectroscopy, and structural analysis using FTIR spectroscopy and elemental analysis.

2.4. Optimization of experimental conditions

2.4.1. Scouting studies and risk assessment. Preliminary scouting experiments were conducted to identify critical factors affecting the fluorescence quenching efficiency and establish appropriate factor ranges for systematic optimization. Initial screening involved one-factor-at-a-time (OFAT) experiments to evaluate the influence of solution pH (2.0–10.0), B,N CQDs concentration (10–150 μg mL^{-1}), and reaction time (1–30 minutes) on analytical performance. Risk assessment was performed to identify potential sources of variability and ensure robust method development.

Based on scouting results and risk analysis, three critical factors were selected for systematic optimization using Box–Behnken response surface methodology. The factor ranges were determined from preliminary studies and are presented in Table S1, ensuring adequate response coverage while maintaining analytical feasibility.

2.4.2. Box–Behnken experimental design. Systematic optimization of the fluorescence quenching conditions was performed using Box–Behnken response surface methodology with three independent variables: solution pH (X_1: 3.0–9.0), B,N CQDs concentration (X_2: 30–90 μg mL^{-1}), and reaction time (X_3: 3.0–10.0 minutes). The experimental ranges were selected based

on scouting studies and are detailed in Table S1. The quenching efficiency (F_0/F) served as the response variable where F_0 and F represent the fluorescence intensities of B,N CQDs in the absence and presence of lisinopril, respectively.

A total of 17 experimental runs were performed according to the Box–Behnken design matrix, including 5 center point replicates to estimate experimental error. Statistical analysis and model validation were conducted using Design Expert software (version 11, Stat-Ease Inc.). Analysis of variance (ANOVA) was employed to evaluate model significance and identify the most influential factors affecting analytical performance.

2.5. General analytical procedure

The optimized analytical protocol proceeded as follows: appropriate aliquots of lisinopril standard or sample solutions containing 0.2–20.0 μg were transferred to 10 mL volumetric flasks to give final concentrations of 0.02–2.0 μg mL^{-1}. Britton–Robinson buffer (1.0 mL, pH 6.7 ± 0.05) was added to each flask, followed by 0.7 mL of B,N CQDs working solution (1 mg mL^{-1}). The solutions were mixed gently and allowed to equilibrate for 3 min at room temperature to ensure complete interaction between the analyte and fluorescent probe. The volumes were adjusted to the mark with deionized water, and the solutions were mixed thoroughly by inversion. Fluorescence measurements were performed immediately after preparation using excitation at 360 nm and monitoring emission at 429 nm. Blank solutions containing all reagents except lisinopril were prepared simultaneously under identical conditions.

2.6. Real sample analysis

2.6.1. Pharmaceutical formulation analysis. Ten tablets of Zestril® (each containing 10 mg lisinopril) were accurately weighed and ground to a fine powder using a mortar and pestle. A portion of powder equivalent to 10 mg lisinopril was accurately weighed and transferred to a 100 mL volumetric flask. The powder was extracted with 50 mL of distilled water using ultrasonication for 20 minutes at room temperature.

The volume was completed to the mark with the same solvent, and the solution was filtered through Whatman No. 42 filter paper to remove insoluble excipients. Appropriate aliquots of the filtrate were further diluted with deionized water to obtain concentrations within the validated linearity range and analyzed according to the general procedure.

2.6.2. Biological sample analysis. Plasma samples were thawed at room temperature and vortexed for 30 seconds before analysis. Aliquots of drug-free plasma were spiked with known concentrations of lisinopril standard solution to achieve final concentrations of 0.05, 0.1, 0.5, 1.0, and 1.5 μg mL^{-1}. Protein precipitation was performed by adding 3.0 mL of ice-cold acetonitrile to each plasma sample. The mixtures were vortexed vigorously for 2 minutes and centrifuged at 4000 rpm for 10 minutes at 4 °C. The clear supernatants were carefully separated and evaporated to dryness under a gentle nitrogen stream at 40 °C. The dried residues were reconstituted with 1.0 mL of distilled water (vortexed for 1 minute, and filtered through 0.22 μm syringe filters then the general analytical procedure described earlier were applied using matrix-matched calibration standards.

2.7. Quantum mechanical studies

Theoretical calculations were performed using Gaussian 09 software package to investigate the molecular interactions between B,N CQDs and lisinopril at the quantum mechanical level. Geometry optimization and frequency calculations were conducted using the PM6 semiempirical method, which provides reliable results for large molecular systems while maintaining computational efficiency.

For theoretical modeling purposes, a representative fragment of the B,N CQDs structure was constructed to maintain computational efficiency while preserving the essential electronic and structural features. The model fragment included the core aromatic system with boron and nitrogen heteroatoms, along with representative surface functional groups such as carboxyl (–COOH) and hydroxyl (–OH) groups that reflect the experimental synthesis conditions and characterization results. Interaction energies between B,N CQDs and lisinopril were calculated using the supermolecular approach:

$$\Delta E = E(\text{complex}) - E(\text{B,N CQDs}) - E(\text{lisinopril}) \quad (1)$$

where E(complex), E(B,N CQDs), and E(lisinopril) represent the total energies of the optimized complex, B,N CQDs, and lisinopril, respectively.

3. Results and discussion

3.1. Characterization and optical properties of B,N CQDs

Comprehensive physicochemical characterization confirmed the successful synthesis of high-quality B,N CQDs with desirable analytical properties. DLS analysis revealed that the synthesized B,N CQDs exhibited uniform size distribution with mean particle diameter of 3.97 nm and standard deviation of 1.48 nm (Fig. 1A). Subsequently, TEM analysis confirmed the monodisperse nature of the nanoparticles, revealing spherical morphology with well-defined boundaries and uniform contrast distribution (Fig. 1B). This narrow size distribution is particularly crucial for consistent optical properties and analytical reproducibility.[21] Complementary structural characterization by FTIR spectroscopy (Fig. 1C) revealed characteristic functional groups that suggested successful surface functionalization and heteroatom incorporation during the thermal synthesis process. Specifically, the broad absorption band at 3200–3600 cm^{-1} was attributed to O–H and N–H stretching vibrations, confirming the presence of hydroxyl and amino groups on the CQDs surface as expected from citric acid and urea precursors. The peak at approximately 1650 cm^{-1} corresponds to C=O stretching vibrations, which could arise from multiple carbonyl-containing functionalities including carboxylic acids, ketones, lactones, or amide groups formed during the hydrothermal synthesis process. The complex surface chemistry of thermally synthesized carbon quantum dots typically encompasses various oxygen-containing functionalities, making definitive assignment challenging based solely on

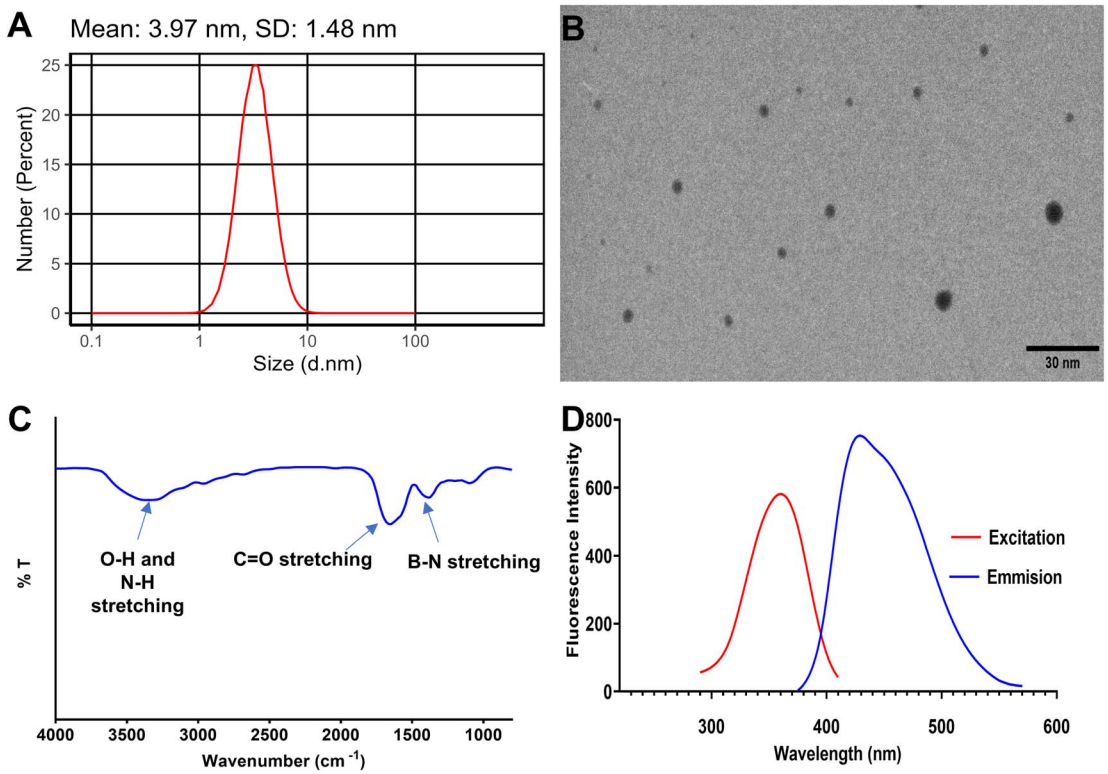

Fig. 1 Physicochemical and optical characterization of synthesized B,N-CQDs. (A) Dynamic light scattering size distribution showing mean particle diameter of 3.97 nm with standard deviation of 1.48 nm. (B) Transmission electron microscopy image revealing spherical morphology with uniform contrast distribution (scale bar: 30 nm). (C) FTIR spectrum displaying characteristic functional groups including O–H and N–H stretching, C=O stretching, and B–N stretching vibrations. (D) Excitation (red line, $\lambda_{em} = 429$ nm) and emission (blue line, $\lambda_{ex} = 360$ nm) spectra demonstrating intense blue fluorescence with large Stokes shift of 69 nm.

vibrational spectroscopy. The characteristic peak observed at 1380 cm^{-1} has been consistently assigned to B–N stretching vibrations in boron–nitrogen co-doped carbon materials according to established literature. Chen *et al.* reported B–N in-plane tensile vibrations at 1371 cm^{-1} in B,N-doped graphene synthesized under hydrothermal conditions,[28] while Ren *et al.* demonstrated that the peak at 1370 cm^{-1} is attributed to symmetric stretching of BN bonds in boron oxynitride systems.[29] These surface functional groups are essential for enhancing water solubility and facilitating molecular interactions with target analytes. Additionally, CHN elemental analysis provided quantitative evidence for successful nitrogen incorporation into the carbon quantum dot framework. The elemental composition revealed: carbon (68.25%), hydrogen (4.12%), and nitrogen (11.84%), with oxygen and boron accounting for the remaining composition (15.79% by difference). The substantial nitrogen content of 11.84% falls within the typical range reported for N-doped carbon quantum dots and demonstrates efficient nitrogen incorporation during the hydrothermal synthesis process using urea as nitrogen source. While CHN analysis cannot directly quantify boron content, the combination of characteristic FTIR signatures at 1380 cm^{-1} (consistent with literature reports for B–N vibrations), enhanced optical properties, and synthesis methodology using boric acid provides supportive evidence for boron incorporation alongside the quantitatively confirmed nitrogen doping.

The optical characterization studies demonstrated that the B,N CQDs possessed superior photophysical properties arising from heteroatom doping effects. Initially, the UV-visible absorption spectrum (Fig. S1) revealed a strong absorption below 250 nm with high intensity (absorbance ~3.0) attributed to π–π* transitions of the aromatic carbon framework, along with a secondary absorption band centered around 330 nm with moderate intensity (absorbance ~0.8) corresponding to *n*–π* transitions involving nitrogen lone pairs and defect states introduced by heteroatom doping.[24] Subsequently, the fluorescence properties were evaluated through excitation-emission spectroscopy (Fig. 1D), which demonstrated that upon excitation at 360 nm, the B,N CQDs exhibited intense blue fluorescence with maximum emission at 429 nm, resulting in a large Stokes shift of 69 nm that effectively minimizes interference from scattered excitation light. The 30 nm red shift from absorption maximum (330 nm) to optimal excitation wavelength (360 nm) is characteristic of heteroatom-doped carbon quantum dots, arising from *n*–π trap-state transitions involving lone-pair electrons on boron and nitrogen dopants and surface-defect emissive states that are optimally populated at longer excitation wavelengths. Notably, the quantum yield was calculated to be 64.2% using quinine sulfate as the reference, representing a significant enhancement compared to undoped CQDs due to the synergistic electronic effects of boron and nitrogen co-doping.[30] These robust optical properties,

combined with excellent photostability, make the synthesized B,N CQDs particularly suitable for analytical applications requiring consistent fluorescence response.

3.2. Fluorescence quenching mechanism

The interaction between B,N CQDs and lisinopril was systematically investigated to elucidate the underlying quenching mechanism and establish the theoretical basis for the developed analytical method. The fluorescence emission spectra demonstrated a progressive decrease in fluorescence intensity upon increasing lisinopril concentrations from 0 to 2 μg mL^{-1} (Fig. 2A), indicating effective quenching of the B,N CQDs fluorescence by the target analyte. This concentration-dependent quenching behavior served as the basis for quantitative determination of lisinopril and warranted comprehensive mechanistic investigation to optimize analytical performance.

Initially, the possibility of inner filter effect was evaluated through UV-visible absorption analysis of lisinopril. The absorption spectrum of lisinopril (Fig. S2) revealed negligible absorption above 250 nm with virtually no measurable absorbance in the excitation and emission wavelength regions of the B,N CQDs. This absence of spectral overlap effectively excluded the inner filter effect as the primary quenching mechanism, thereby confirming that the observed fluorescence quenching resulted from genuine molecular interactions between the fluorophore and analyte.

Subsequently, Stern–Volmer analysis was conducted to quantify the quenching efficiency and determine the nature of the interaction mechanism (Fig. 2B). The linear Stern–Volmer plots at three different temperatures (298, 303, and 313 K) yielded Stern–Volmer constants (K_{sv}) of 7.94×10^5, 7.11×10^5, and 5.48×10^5 M^{-1}, respectively (Table 1). Notably, the K_{sv} values demonstrated a systematic decrease with increasing temperature, which is characteristic of static quenching mechanisms rather than dynamic collisional quenching.[31] To further validate this conclusion, the bimolecular quenching rate constants (K_q) were calculated using the relationship:

$$K_q = K_{sv}/\tau_0 \quad (2)$$

where τ_0 represents the fluorescence lifetime of B,N CQDs in the absence of quencher. Considering the typical fluorescence lifetime of carbon quantum dots in the nanosecond range (5–10 ns), the calculated K_q values ranged from 10^{13} to 10^{14} $M^{-1}s^{-1}$, which significantly exceed the diffusion-controlled limit (10^{10} $M^{-1}s^{-1}$) for dynamic quenching in aqueous solutions. These findings provide compelling evidence for a static quenching mechanism involving ground-state complex formation between B,N CQDs and lisinopril.

Furthermore, the binding constants (K_a) were determined using the modified Stern–Volmer equation for static quenching:

$$F_0/F_0 - F = 1/K_a[Q] + 1/K_a \quad (3)$$

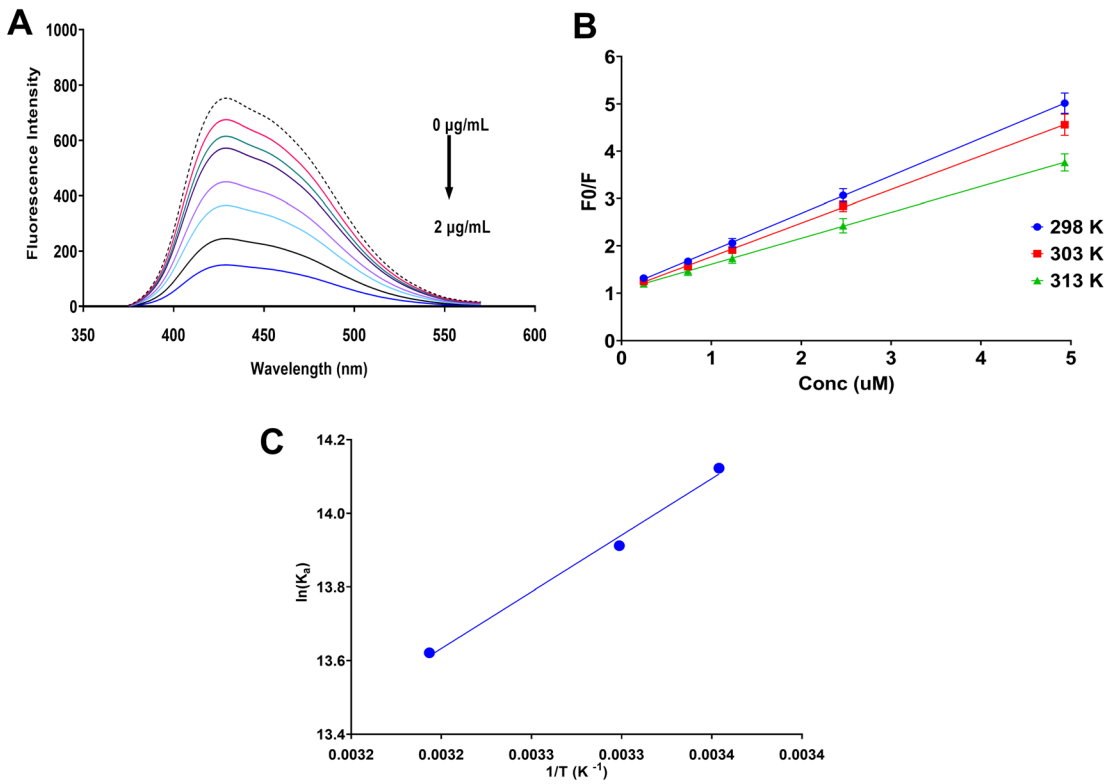

Fig. 2 (A) Fluorescence emission spectra of B,N-CQDs (70 μg mL^{-1}) upon increasing lisinopril concentrations from 0 to 2.0 μg mL^{-1} at pH 6.7, demonstrating progressive quenching with concentration-dependent behavior. (B) Stern–Volmer plots at three different temperatures (298 K, 303 K, 313 K) showing linear relationships with decreasing K_{sv} values at higher temperatures, indicating static quenching mechanism. (C) Van't Hoff plot (ln K_a *vs.* 1/T) used for determination of thermodynamic parameters.

Table 1 Thermodynamic and kinetic parameters for B,N-CQDs-lisinopril interaction at different temperatures

Temperature (K)	K_{sv} (10^5 M^{-1})	K_a (10^6 M^{-1})	ΔG (kJ mol^{-1})	ΔH (kJ mol^{-1})	ΔS (J mol^{-1} K^{-1})
298	7.94	1.36	−35.01	−26.00	30.21
303	7.11	1.10	−35.06		
313	5.48	0.82	−35.46		

where F_0 and F represent the fluorescence intensities in the absence and presence of quencher, respectively. The calculated K_a values were 1.36×10^6, 1.10×10^6, and 0.82×10^6 M^{-1} at 298, 303, and 313 K, respectively (Table 1). The substantial magnitude of these binding constants indicates strong affinity between B,N CQDs and lisinopril, while their temperature-dependent decrease further supports the static quenching mechanism.

The thermodynamic parameters provided additional insights into the nature of the binding interaction (Table 1) as analyzed using the van't Hoff plot (Fig. 2C). The negative Gibbs free energy values ($\Delta G = -35.01$, -35.06, and -35.46 kJ mol^{-1} at 298, 303, and 313 K, respectively) confirmed the spontaneous nature of the binding process. The negative enthalpy change ($\Delta H = -26.00$ kJ mol^{-1}) suggested that the interaction was exothermic and primarily driven by van der Waals forces and hydrogen bonding. Additionally, the positive entropy change ($\Delta S = 30.21$ J mol^{-1} K^{-1}) indicated increased randomness upon complex formation, likely due to the release of bound water molecules from the interaction sites.[33] These thermodynamic signatures are consistent with a static quenching mechanism involving hydrogen bonding and electrostatic interactions between the amino and carboxyl groups of lisinopril and the surface functional groups of B,N CQDs, as evidenced by the FTIR characterization results.

3.3. Quantum mechanical studies

Theoretical calculations were performed to provide molecular-level insights into the interaction mechanism between B,N-CQDs and lisinopril, based on a computational model consistent with experimental FTIR evidence. PM6 semiempirical method was selected due to its improved parameterization for heteroatom-containing systems, particularly boron and nitrogen, compared to earlier semiempirical methods. Additionally, the relatively large size of the B,N-CQDs fragment model necessitated a computationally efficient approach that could provide reasonable accuracy for binding energy calculations while remaining computationally feasible for the systematic studies performed. For theoretical modeling purposes, a representative fragment of the B,N-CQDs structure was constructed based on comprehensive experimental characterization evidence. The model structure selection was guided by FTIR spectroscopic data showing characteristic B–N stretching vibrations at 1380 cm^{-1}, CHN elemental analysis confirming nitrogen incorporation (11.84%), and synthesis methodology employing boric acid and urea as heteroatom sources. The model fragment included the core aromatic carbon system with boron atoms directly bonded to nitrogen atoms, consistent with the literature-supported assignment of B–N stretching vibrations. Representative surface functional groups such as carboxyl (–COOH) and hydroxyl (–OH) groups were incorporated based on FTIR evidence, reflecting the experimental synthesis conditions and characterization results. This computational model represents a theoretical framework constructed to be consistent with experimental evidence rather than a definitive structural determination.

Geometry optimization using the PM6 semiempirical method yielded stable structures for both the individual components and their complex (Fig. 3). The optimized structure of lisinopril (Fig. 3A) demonstrated a total energy of −0.350620 hartree, while the B,N CQDs fragment (Fig. 3B) exhibited a slightly lower energy of −0.434781 hartree, indicating the inherent stability of both molecular systems. Subsequently, the optimized complex formation (Fig. 3C) resulted in a total energy of −0.798190 hartree, representing the energetically favorable binding configuration between the fluorophore and analyte.

The binding energy (ΔE) was calculated using the supermolecular approach according to eqn (1), yielding a value of −0.012789 hartree, which converts to −33.58 kJ mol^{-1} for the complex formation. This negative binding energy confirmed the thermodynamically favorable interaction between B,N CQDs and lisinopril, which correlates excellently with the experimentally determined Gibbs free energy values ($\Delta G = -35.01$ to -35.46 kJ mol^{-1}) obtained from the thermodynamic analysis, with less than 5% deviation. The outstanding agreement between theoretical and experimental values validates the computational model and demonstrates that the PM6 method adequately captures the essential binding interactions, despite the simplified model system and gas-phase calculations.

Detailed analysis of the optimized complex geometry revealed two distinct electrostatic interaction sites that govern the binding mechanism (Fig. 3C). The first interaction site involves the amino group of lisinopril and the carboxylic acid functional group of the B,N CQDs, with an intermolecular distance of 4.4 Å. This relatively short distance indicates strong interaction, which is consistent with the negative enthalpy change ($\Delta H = -26.00$ kJ mol^{-1}) observed experimentally and supports the proposed electrostatic bonding mechanism. The second interaction site occurs between the carboxylic acid group of lisinopril and a boron atom in the B,N CQDs framework, characterized by an intermolecular distance of 3.6 Å. This interaction represents a Lewis acid–base interaction where the electron-deficient boron atom acts as an electron acceptor for the oxygen lone pairs of the carboxylic group. This quantum mechanical calculations further revealed that the boron and

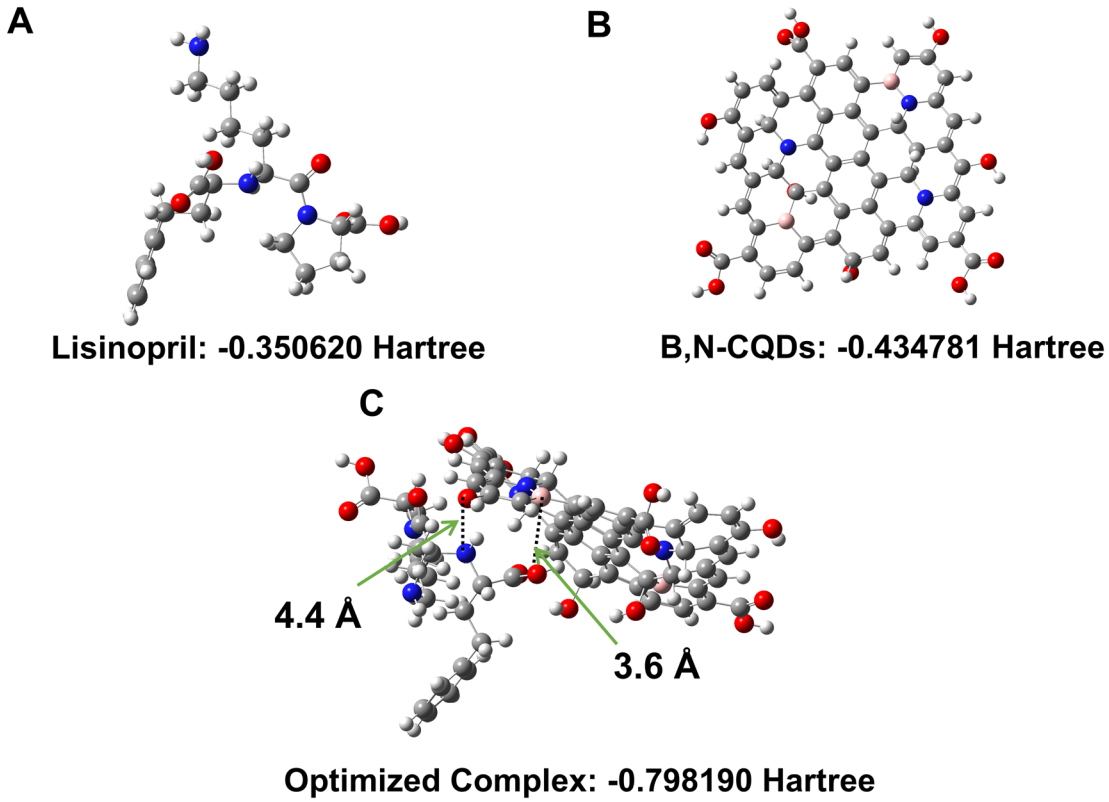

Fig. 3 Quantum mechanical study of B,N-CQDs and lisinopril interaction. (A) Optimized structure of lisinopril molecule (total energy: −0.350620 hartree). (B) Optimized structure of B,N-CQDs fragment model (total energy: −0.434781 hartree). (C) Optimized complex geometry showing binding configuration between B,N-CQDs and lisinopril (total energy: −0.798190 hartree) with two electrostatic interaction sites: amino group of lisinopril with carboxylic group of B,N-CQDs (4.4 Å) and carboxylic group of lisinopril with boron atom of B,N-CQDs (3.6 Å).

nitrogen co-doping significantly enhances the selectivity of the B,N CQDs toward both the acidic and basic functional groups present in lisinopril. The incorporation of boron atoms creates electron-deficient sites within the carbon framework, thereby increasing the affinity for electron-rich functional groups such as carboxylic acids. This synergistic effect of heteroatom doping explains the superior analytical performance of B,N CQDs compared to undoped carbon quantum dots and provides a rational basis for the high selectivity observed in the experimental studies. Furthermore, the computational results validate the static quenching mechanism by demonstrating that stable ground-state complexes can form between B,N CQDs and lisinopril through multiple complementary interaction sites, as evidenced by the favorable binding energetics and optimal intermolecular geometries.

3.4. Optimization of experimental conditions

Systematic optimization of the experimental conditions was conducted using Box–Behnken response surface methodology to maximize the fluorescence quenching efficiency and establish robust analytical performance. Box–Behnken design is a response surface methodology that uses a three-level factorial approach to efficiently explore the relationship between multiple independent variables and the response through strategically positioned experimental points. This design offers significant advantages over traditional one-factor-at-a-time approaches by requiring fewer experimental runs while maintaining statistical validity for estimating quadratic response surfaces and factor interactions. The experimental design matrix (Table S1) encompassed three critical factors: solution pH (A: 3.0–9.0), B,N CQDs concentration (B: 30–90 μg mL^{-1}), and reaction time (C: 3.0–10.0 minutes), with quenching efficiency (QE%) serving as the response variable. Analysis of variance (ANOVA) demonstrated the statistical significance of the developed model (Table 2) with F-value of 49.69 and p-value < 0.0001, confirming that the model adequately describes the experimental data and can be used for optimization purposes. The lack of fit was not significant ($p = 0.1901$), indicating that the model fits the experimental data well without systematic error, while the pure error component validates the reproducibility of the experimental measurements.

The mathematical relationship between the response variable and the independent factors was expressed through the following coded equation derived from multiple regression analysis:

$$\mathrm{QE\%} = 2.96213 + 0.231511 \times A + 0.414689 \times B + 0.19792 \times \mathrm{AB} - 0.686 \times A^2 - 0.589935 \times B^2 \quad (4)$$

where A and B represent the coded values of pH and B,N CQDs concentration, respectively. The positive linear coefficients for

Table 2 Analysis of variance (ANOVA) for Box–Behnken response surface model showing statistical significance of factors affecting fluorescence quenching efficiency

Source	Sum of squares	df	Mean square	*F*-value	*p*-value	
Model	5.62	5	1.12	49.69	<0.0001	Significant
A-pH	0.4288	1	0.4288	18.96	0.0011	
B-B,N-doped CQDs conc.	1.38	1	1.38	60.83	<0.0001	
AB	0.1567	1	0.1567	6.93	0.0233	
A^2	1.99	1	1.99	87.86	<0.0001	
B^2	1.47	1	1.47	64.97	<0.0001	
Residual	0.2488	11	0.0226			
Lack of fit	0.2034	7	0.0291	2.56	0.1901	Not significant
Pure error	0.0454	4	0.0113			
Cor total	5.87	16				

pH (0.231511) and B,N CQDs concentration (0.414689) indicate that increasing these factors enhances the quenching efficiency within the studied ranges. Notably, the B,N CQDs concentration exhibits the largest linear coefficient, suggesting its dominant influence on analytical performance. The positive interaction coefficient (AB = 0.19792) reveals synergistic effects between pH and B,N CQDs concentration, indicating that the optimal response requires simultaneous optimization of both factors. Conversely, the negative quadratic coefficients for pH ($A^2 = -0.686$) and B,N CQDs concentration ($B^2 = -0.589935$) confirm the existence of optimal points rather than linear relationships, supporting the curvature observed in the response surface plots.

Model adequacy was rigorously evaluated through comprehensive statistical analysis (Table S2 and Fig. S3–S4). The coefficient of determination ($R^2 = 0.9576$) indicated that 95.76% of the variability in quenching efficiency can be explained by the model, while the adjusted R^2 (0.9383) accounts for the number of terms in the model and confirms excellent fit quality. The predicted R^2 (0.8429) demonstrates satisfactory predictive capability, with the difference between adjusted and predicted R^2 being less than 0.2, indicating good model stability. Furthermore, the adequate precision value of 19.2989 significantly exceeds the minimum threshold of 4.0, confirming that the model has sufficient signal-to-noise ratio for reliable optimization. The coefficient of variation (6.37%) falls within acceptable limits, indicating good reproducibility of the experimental measurements. Diagnostic plots (Fig. S3) including normal probability plots, predicted *versus* actual values, and residual analyses demonstrated random distribution of residuals without systematic patterns, confirming the validity of the regression assumptions. The run order analysis (Fig. S4A) demonstrated random distribution of residuals across the experimental sequence with no systematic trends, confirming the absence of time-dependent effects such as instrument drift or reagent degradation during the experimental campaign. Additionally, the leverage analysis (Fig. S4B) showed that all experimental points fell within acceptable limits, indicating that the experimental design was well-balanced and no individual runs exerted confirming no influence on the model parameters, further validating the model robustness and reliability.

The main effect plots (Fig. 4) provided comprehensive insights into the individual factor influences on quenching efficiency, directly correlating with the mathematical coefficients in eqn (4). The pH effect (Fig. 4A) demonstrated a clear optimum around pH 6.7, reflecting the complex relation between the protonation states of both the B,N CQDs surface functional groups and lisinopril. At lower pH values, excessive protonation leads to aggregation of B,N CQDs due to reduced electrostatic repulsion between particles. Conversely, at higher pH values, deprotonation of the amino group in lisinopril prevents its effective interaction with the negatively charged surface of deprotonated B,N CQDs, leading to electrostatic repulsion rather than attraction. This pH dependence aligns with the negative quadratic coefficient ($A^2 = -0.686$) and explains the parabolic relationship observed experimentally. The B,N CQDs concentration effect (Fig. 4B) showed increasing quenching efficiency up to approximately 72 μg mL^{-1}, beyond which a plateau was observed. This behavior reflects the saturation of available binding sites and is consistent with the positive linear coefficient (0.414689) and negative quadratic term (−0.589935). The reaction time effect (Fig. 4C) indicated rapid equilibration within 3 min, suggesting efficient complex formation kinetics that support the static quenching mechanism established in the mechanistic studies. Notably, reaction time was found to be statistically non-significant ($p > 0.05$) in the ANOVA analysis and was consequently excluded from the reduced quadratic model equation. This exclusion confirms that the binding equilibrium is rapidly achieved and that reaction time does not significantly influence the analytical response within the studied range, thereby simplifying the optimization process to focus on the two critical factors: pH and B,N CQDs concentration.

The interaction and three-dimensional response surface plots (Fig. S5) revealed the synergistic relation between pH and B,N CQDs concentration, as quantified by the positive interaction coefficient (AB = 0.19792). The two-dimensional interaction plot (Fig. S5A) demonstrated curved response lines at different B,N CQDs concentrations, indicating that optimal quenching efficiency requires simultaneous optimization of both factors rather than individual factor optimization. The three-dimensional response surface plot (Fig. S5B) clearly visualized the response maximum as a distinct peak in the

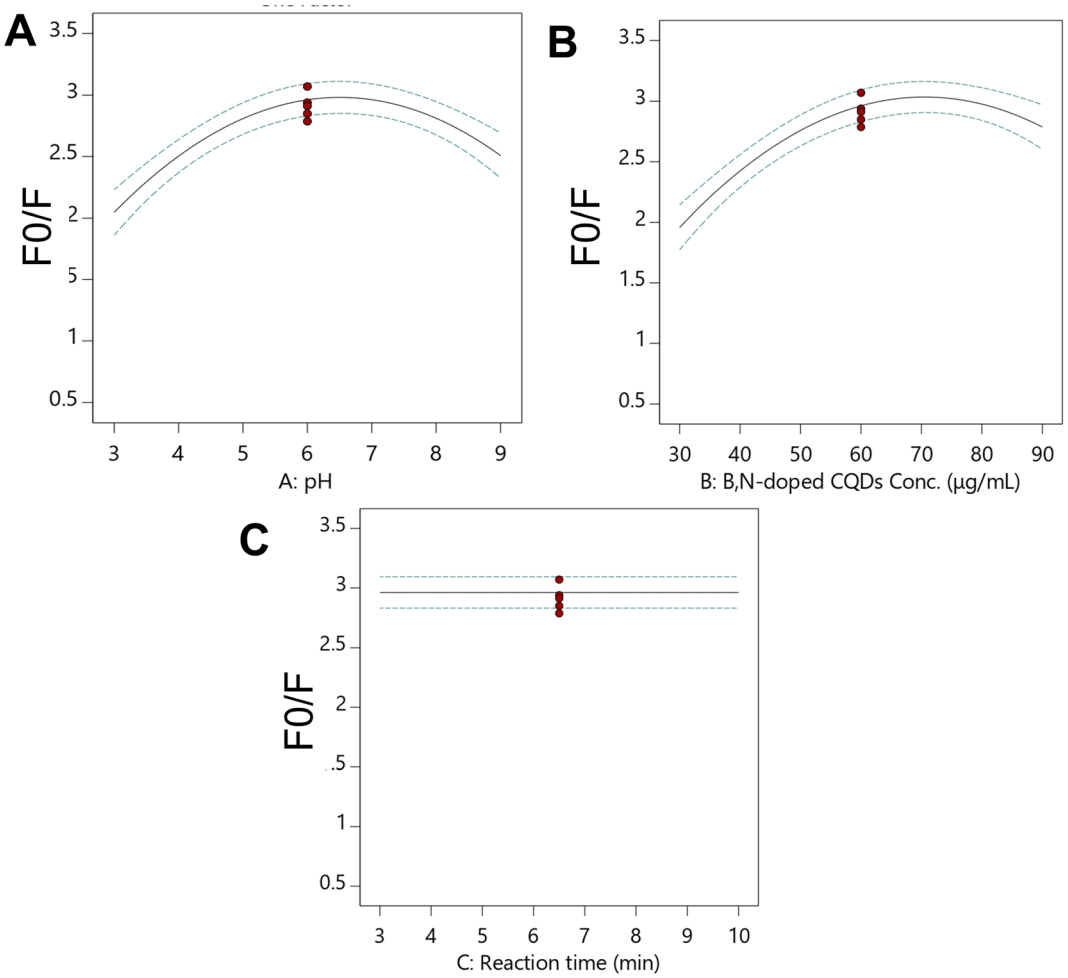

Fig. 4 Main effect plots from Box–Behnken optimization showing individual factor influences on quenching efficiency (F_0/F). (A) Effect of pH demonstrating optimal quenching at pH 6–7 due to balanced protonation states of B,N CQDs and lisinopril. (B) Effect of B,N CQDs concentration showing increasing quenching efficiency up to 70–75 µg mL^{-1} followed by plateau due to binding site saturation. (C) Effect of reaction time indicating rapid equilibration within 3 minutes, supporting static quenching mechanism and confirming non-significance of this factor in the final model.

surface, confirming the existence of well-defined optimal conditions at approximately pH 6.7 and B,N CQDs concentration of 72 µg mL^{-1}. This synergistic behavior can be attributed to the pH-dependent surface charge of B,N CQDs, which affects the accessibility and reactivity of functional groups toward lisinopril binding. At the optimal pH, the B,N CQDs surface exhibits balanced protonation states that maximize both hydrogen bonding and electrostatic interactions, while sufficient concentration ensures adequate probe availability for complex formation.

Numerical optimization using the desirability function approach (Fig. S6) identified the optimal conditions as pH 6.68, B,N CQDs concentration 71.68 µg mL^{-1}, and reaction time 3.12 minutes, yielding a predicted maximum quenching efficiency of 3.07. For practical analytical applications, these conditions were approximated to pH 6.7 ± 0.05, B,N CQDs concentration 70 µg mL^{-1}, and reaction time 3 minutes, which provide convenient working parameters while maintaining optimal analytical performance. The excellent agreement between predicted and experimental values under these optimized conditions validates the model reliability and demonstrates the successful application of response surface methodology for method development. These optimized parameters were subsequently employed for all validation studies and real sample analyses, ensuring consistent and maximum analytical sensitivity throughout the investigation.

3.5. Method validation and selectivity studies

Comprehensive method validation was conducted according to ICH Q2(R2) guidelines[32] to establish the analytical performance characteristics of the developed fluorescence quenching method (Table 3). The method demonstrated excellent linearity over the concentration range of 0.02–2.0 µg mL^{-1} with a correlation coefficient (r^2) of 0.9998, indicating strong linear relationship between fluorescence quenching and lisinopril concentration. The limits of detection (LOD) and quantification (LOQ) were calculated as 6.21 ng mL^{-1} and 18.63 ng mL^{-1}, respectively, using the standard deviation of the blank and

Table 3 Analytical performance parameters for the validated B,N-CQDs fluorescence quenching method according to ICH Q2(R2) guidelines

Parameters		Lisiopril
Excitation wavelength (nm)		360
Emission wavelength (nm)		429
Linearity range (μg mL^{-1})		0.02–2.0
Slope		1.9580
Intercept		1.0998
Correlation coefficient (r^2)		0.9998
LOD (ng mL^{-1})		6.21
LOQ (ng mL^{-1})		18.63
Accuracy (% R)[a]		98.14 ± 0.857
Repeatability precision (% RSD)[b]		0.873
Intermediate precision (% RSD)[c]		1.244
Robustness (% R)	Buffer (pH)	101.80 ± 1.397
	Reagent conc. (μg mL^{-1})	98.90 ± 0.804
	Reaction time (min)	100.68 ± 0.889

[a] Average of 9 determinations (3 concentrations repeated 3 times). [b] % RSD of 9 determinations (3 concentrations repeated 3 times) measured on the same day. [c] % RSD of 9 determinations (3 concentrations repeated 3 times) measured in the three consecutive days.

slope approach (LOD = $3.3\sigma/S$, LOQ = $10\sigma/S$). These detection limits demonstrate superior sensitivity compared to many existing analytical methods for lisinopril determination and enable quantification at therapeutically relevant concentrations in biological matrices.

The accuracy evaluation revealed excellent recovery with an overall accuracy of 98.14 ± 0.857% based on nine determinations across three concentration levels, confirming minimal systematic bias in the analytical procedure (Table 3). Precision studies demonstrated satisfactory reproducibility with repeatability precision (intra-day) of 0.873% RSD and intermediate precision (inter-day) of 1.244% RSD, both well within the acceptable limits for pharmaceutical analysis (<2% RSD). Robustness evaluation assessed the method's resistance to small variations in critical parameters, yielding recoveries of 101.80 ± 1.397% for buffer pH variations, 98.90 ± 0.804% for reagent concentration changes, and 100.68 ± 0.889% for reaction time modifications. These results confirm that minor analytical variations do not significantly affect method performance, supporting the method's reliability for routine analytical applications.

Selectivity studies (Fig. S7) demonstrated the method's high performance for lisinopril determination in the presence of potential interferents commonly found in pharmaceutical formulations and biological matrices. While lisinopril exhibited remarkable quenching efficiency of approximately 67%, all tested interferents including inorganic salts (Na^+, K^+, Ca^{2+}, Mg^{2+}), transition metals (Ni^{2+}, Cd^{2+}), anions (SO_4^{2-}, PO_4^{3-}), excipients (starch, lactose, cellulose, magnesium stearate, sodium lauryl sulfate) and biological components (tryptophan, tyrosine, glutamic acid, glucose) showed negligible interference with quenching efficiencies below 5%. Importantly, structurally similar ACE inhibitors including captopril, enalapril, and ramipril demonstrated significantly lower quenching efficiencies (below 5%) compared to lisinopril despite their structural similarities, confirming excellent method selectivity even against closely related compounds. This high selectivity can be attributed to the specific interaction mechanism between B,N CQDs and the unique structural features of lisinopril, particularly its amino and carboxylic acid functional groups that enable optimal binding geometry as confirmed by quantum mechanical calculations.

The comprehensive validation study establishes that the developed B,N CQDs fluorescence quenching method meets all ICH requirements for pharmaceutical analysis with superior analytical performance characteristics. The combination of excellent linearity, high sensitivity, satisfactory precision and accuracy, robust performance, and high selectivity makes this method highly suitable for quantitative determination of lisinopril in pharmaceutical formulations and biological samples, offering significant advantages over existing analytical approaches in terms of simplicity and cost-effectiveness.

3.6. Application of the developed method

The practical applicability of the developed B,N CQDs fluorescence quenching method was evaluated through analysis of real pharmaceutical formulations and biological samples to demonstrate its suitability for routine analytical applications. Statistical comparison with a reference HPLC method was conducted to assess method equivalence and establish analytical reliability under real-world conditions.

The method was successfully applied to the determination of lisinopril in commercial tablet formulations (Zestril®, 10 mg) with excellent analytical performance (Table 4). The developed fluorescence method yielded a mean recovery of 100.03 ± 0.724% ($n = 5$), demonstrating high accuracy and precision for pharmaceutical analysis. Statistical comparison with a reference HPLC method[11] showed a mean recovery of 99.69 ± 0.99% for the same tablet samples. The two-tailed t-test (calculated $t = 0.523$) was significantly lower than the tabulated value ($t = 2.306$ at $P = 0.05$), indicating no statistically significant difference between the methods. Similarly, the F-test (calculated $F = 1.873$) was below the critical value ($F = 6.338$ at $P = 0.05$), confirming

Table 4 Statistical comparison between the developed B,N-CQDs fluorescence method and reference HPLC method for lisinopril determination in pharmaceutical formulations

Method	Mean[a]	SD	t-test (2.306)[b]	P value	F-value (6.338)[b]	P value	θ_L[c]	θ_U[c]
Developed method	100.03	0.724	0.523	0.628	0.549	1.873	0.558	−0.920
Reported method	99.69	0.99						

[a] Average of five determinations. [b] The values in parenthesis are tabulated values of "t"and "F" at ($P = 0.05$). [c] Bias of ± 2% is acceptable.

equivalent precision between the methods. The bias evaluation using the ±2% acceptance criterion showed $\theta_L = -0.920$ and $\theta_U = 0.558$, both within acceptable limits, establishing method equivalence and confirming the absence of systematic bias. These results validate the developed method's accuracy and reliability for pharmaceutical quality control applications.

Recovery studies were also conducted using drug-free human plasma spiked with known concentrations of lisinopril to evaluate the method's performance in biological matrices (Table S3). The method demonstrated excellent recovery across the tested concentration range (0.05–1.5 μg mL^{-1}) with recovery percentages ranging from 97.46% to 103.64%. At the lowest concentration (0.05 μg mL^{-1}), the method achieved 97.46% recovery with 3.454% RSD, demonstrating satisfactory performance near the quantification limit. Mid-range concentrations (0.1 and 0.5 μg mL^{-1}) showed optimal performance with recoveries of 103.64% and 102.36%, respectively, and improved precision (RSD < 3%). At the highest concentration (1.5 μg mL^{-1}), the method maintained excellent accuracy (97.81% recovery) with the best precision (1.353% RSD). The consistent recovery values across the concentration range and acceptable precision (RSD < 5%) confirm the method's suitability for bioanalytical applications.

3.7. Greenness and practicality assessment

The comprehensive evaluation of analytical methods requires assessment beyond traditional analytical performance parameters to include environmental impact and practical applicability. To provide a holistic sustainability and practicality evaluation of the developed B,N CQDs fluorescence method for lisinopril determination, four complementary assessment tools were employed: Analytical GREEnness Metric (AGREE),[33] Modified Green Analytical Procedure Index (MoGAPI),[34] Blue Applicability Grade Index (BAGI),[35] and Click Analytical Chemistry Index (CACI).[36] This multi-metric approach ensures

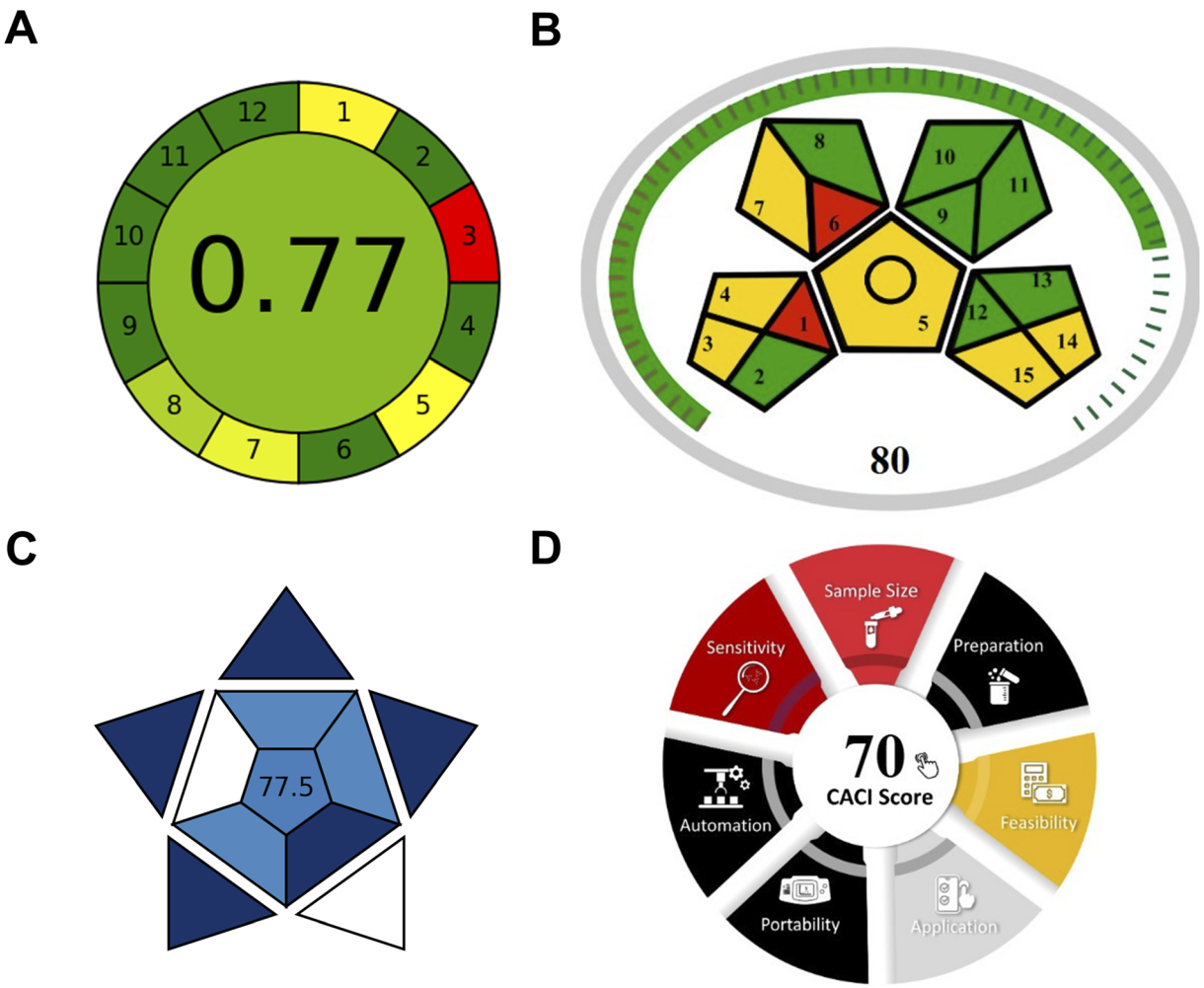

Fig. 5 Comprehensive greenness and practicality assessment of the developed B,N-CQDs fluorescence method using four complementary evaluation metrics. (A) AGREE pictogram demonstrated excellent environmental performance with a score of 0.77. (B) MoGAPI assessment yielded 80% classification as "excellent green" method. (C) BAGI evaluation showed good practical performance with a score of 77.5, confirming quantitative determination capability, rapid sample throughput, and minimal sample preparation requirements. (D) CACI assessment indicated highly practical method performance with a score of 70, demonstrating simplified procedures, high feasibility, and rapid analysis time.

comprehensive evaluation across environmental, practical, and implementation perspectives as summarized in Fig. 5.

3.7.1. Greenness assessment using AGREE and MoGAPI metrics. The AGREE metric, based on the 12 principles of green analytical chemistry (SIGNIFICANCE), transforms assessment criteria into a unified 0–1 scale with results presented as a clock-like pictogram.[33] For the B,N CQDs fluorescence method, the assessment revealed excellent environmental performance with a score of 0.77 (Fig. 5A). The method demonstrated particularly strong performance in (1) minimal sample treatment requiring only simple rxtraction procedures for pharmaceutical formulations and protein precipitation for biological samples without derivatization steps, (2) minimal reagent consumption including 1.0 mL Britton–Robinson buffer and 0.7 mL B,N CQDs solution representing significantly reduced chemical usage compared to conventional chromatographic methods, (3) excellent energy efficiency with fluorescence spectroscopy consuming less than 0.15 kWh per sample through room temperature operation, and (5) reduced waste generation producing minimal aqueous waste (<5 mL per sample) with no organic solvents required for the determination step.

The MoGAPI assessment, which combines the visual impact of GAPI with quantitative total scoring, yielded a score of 80% classifying the method as excellent green (Fig. 5B). The high score reflected (1) off-line sample collection with no preservation requirements and minimal transport considerations, (2) simple analytical procedures without complex extraction requirements operating at room temperature, (3) readily available reagents with B,N CQDs synthesized from commercially available precursors including citric acid, boric acid, and urea using standard laboratory equipment, (4) accessible instrumentation utilizing standard fluorescence spectroscopy equipment available in most analytical laboratories, and (5) minimal environmental impact through reduced waste generation and low energy consumption. The MoGAPI assessment confirmed the method's superior environmental performance compared to conventional analytical approaches for lisinopril determination, particularly highlighting the advantages of green solvent usage and simplified analytical procedures.

3.7.2. Practicality assessment using BAGI and CACI metrics. The BAGI metric evaluates the practicality of analytical methods focusing on practical aspects through assessment of ten main attributes. The developed method achieved a score of 77.5 (Fig. 5C), indicating good practical performance with several strengths. The assessment revealed (1) quantitative determination capability with confirmatory potential through fluorescence spectroscopy providing robust analytical information, (2) rapid sample throughput with 3-minutes analysis time enabling more than 20 samples per hour processing meeting high-throughput laboratory requirements, (3) excellent reagent availability with all required chemicals commercially accessible and simple B,N CQDs synthesis using standard laboratory equipment and (4) minimal sample preparation requirements involving only simple dilution or protein precipitation achieving high practicality scores. Areas identified for potential improvement included (1) expansion from single analyte determination to multi-analyte capability and (2) enhanced automation implementation for fully unattended operation.

The CACI assessment, emphasizing simplicity, efficiency, and reliability inspired by click chemistry principles, resulted in a score of 70 indicating highly practical method performance (Fig. 5D). The evaluation demonstrated excellent alignment with click analytical chemistry principles through (1) simplified sample preparation, (2) excellent feasibility with all reagents commercially available, standard fluorescence instrumentation accessible in most laboratories, and estimated cost less than $10 per sample analysis, (3) quantitative determination capability applicable to pharmaceutical formulations and biological matrices demonstrating analytical versatility, (4) acceptable sensitivity with detection limit of 6.21 ng mL^{-1} representing less than 1% of pharmaceutical concentrations, and (6) rapid analysis time. The CACI assessment confirmed the method's practical advantages including simplicity, cost-effectiveness, and rapid implementation suitable for routine analytical applications.

The comprehensive multi-metric assessment demonstrates that the developed B,N CQDs fluorescence method exhibits excellent environmental traits with high practical applicability. All four metrics consistently identified the method's strengths in environmental sustainability through minimal reagent consumption, absence of organic solvents, low energy requirements, and reduced waste generation, combined with practical implementation advantages including simple procedures, readily available reagents and instrumentation, and rapid analysis times. The assessment scores of AGREE (0.77), MoGAPI (80%), BAGI (77.5), and CACI (70) collectively establish the method as a sustainable and practical alternative for routine lisinopril determination, demonstrating significant improvements over conventional analytical approaches and supporting the transition toward more environmentally responsible analytical practices in pharmaceutical quality control and bioanalytical applications.

4. Conclusion

This study successfully developed and validated a novel fluorescence quenching method for lisinopril determination using B,N-doped carbon quantum dots as fluorescent probes. The synthesized B,N CQDs exhibited uniform morphology with mean diameter of 3.97 nm and superior optical properties, including intense blue fluorescence with excitation maximum at 360 nm and emission at 429 nm. Comprehensive mechanistic investigations through Stern–Volmer analysis, thermodynamic studies, and quantum mechanical calculations confirmed static quenching *via* ground-state complex formation, with Stern–Volmer constants decreasing from 7.94×10^5 to 5.48×10^5 M^{-1} as temperature increased from 298 to 313 K. The quantum mechanical studies revealed binding energy of -33.58 kJ mol^{-1}, demonstrating excellent agreement with experimental thermodynamic parameters ($\Delta G = -35.01$ kJ mol^{-1}). Systematic optimization using Box–Behnken response surface methodology identified optimal conditions of pH 6.7, B,N CQDs concentration 70 μg mL^{-1}, and 3-minutes reaction time. The developed

method demonstrated excellent analytical performance with linear range of 0.02–2.0 μg mL^{-1}, detection limit of 6.21 ng mL^{-1}, and quantification limit of 18.63 ng mL^{-1}. Method validation according to ICH Q2(R2) guidelines confirmed satisfactory accuracy (98.14 ± 0.857%), precision (RSD < 1.25%), and robustness. Successful application to commercial tablet formulations yielded recovery of 100.03 ± 0.724%, while spiked human plasma samples demonstrated excellent recovery ranging from 97.46% to 103.64%. The method offers significant advantages over conventional analytical approaches, including cost-effectiveness through simple reagent requirements, room-temperature operation eliminating thermal control needs, rapid analysis time enabling high sample throughput, and superior environmental profile with comprehensive sustainability assessment scores (AGREE: 0.77, MoGAPI: 80%, BAGI: 77.5, CACI: 70).

Despite the promising analytical performance and practical advantages, several limitations warrant consideration for future development. The primary limitation concerns selectivity challenges when analyzing complex biological matrices containing structurally similar compounds with amino and carboxylic acid functional groups. While the method demonstrated excellent selectivity against tested interferents, the fluorescence quenching mechanism relies on specific interactions between B,N CQDs and lisinopril's functional groups, which may not provide absolute selectivity in the presence of structurally related pharmaceuticals. Future research should focus on enhancing method selectivity through advanced recognition strategies, particularly the development of molecularly imprinted polymers (MIPs) combined with B,N CQDs. MIP-CQDs composite materials could provide dual recognition mechanisms, combining the fluorescence properties of B,N CQDs with the selective binding cavities of molecularly imprinted polymers, thereby significantly improving selectivity against structurally similar interferents. Additionally, surface modification of B,N CQDs with specific recognition elements or aptamers could enhance selectivity while maintaining excellent analytical performance. Integration with advanced separation techniques such as capillary electrophoresis or microfluidic devices could provide additional selectivity dimensions, while extending the method to simultaneous determination of multiple ACE inhibitors through multivariate calibration approaches would increase practical applicability. This work represents a significant advancement in pharmaceutical analysis, offering a sustainable, cost-effective, and sensitive alternative for lisinopril determination with promising potential for further development in bioanalytical applications.

Conflicts of interest

There are no conflicts of interest to declare.

Data availability

The authors confirm that the data supporting the findings of this study are available within the article and its supplementary information file (SI). Supplementary information is available. See DOI: https://doi.org/10.1039/d5ra05164a.

Acknowledgements

This research was funded by Deanship of Research and Graduate Studies at King Khalid University, Saudi Arabia, Project No. (RGP2/384/46). The authors extend their appreciation to the Deanship of Research and Graduate Studies at King Khalid University for funding this work through Large Research Project under grant number RGP2/384/46.

References

1 M. Sobhy, A. Eletriby, H. Ragy, H. Kandil, M. A. Saleh, N. Farag, R. Guindy, A. Bendary, A. M. E. Nayel, A. Shawky, A. Khairy, A. Mortada, B. Zarif, H. Badran, H. Khorshid, K. Mahmoud, K. Said, K. Leon, M. Abdelsabour, M. Tawfik, M. A.-K. F. Abdelmegid, M. Koriem, M. Loutfi, M. Wadie, M. Elnoamany, M. Sadaka, M. Seleem, M. Zahran, O. A. Amin, S. Elkaffas, S. Ayad, W. E. Kilany, W. Ammar, W. Elawady, W. Elhammady and Y. Abdelhady, *Cardiol. Ther.*, 2024, **13**, 707–736.
2 L. C. van Vark, M. Bertrand, K. M. Akkerhuis, J. J. Brugts, K. Fox, J.-J. Mourad and E. Boersma, *Eur. Heart J.*, 2012, **33**, 2088–2097.
3 R. Chen, M. A. Suchard, H. M. Krumholz, M. J. Schuemie, S. Shea, J. Duke, N. Pratt, C. G. Reich, D. Madigan, S. C. You, P. B. Ryan and G. Hripcsak, *Hypertension*, 2021, **78**, 591–603.
4 F. H. Messerli, S. Bangalore, C. Bavishi and S. F. Rimoldi, *J. Am. Coll. Cardiol.*, 2018, **71**, 1474–1482.
5 J. Wong, R. A. Patel and P. R. Kowey, *Progress in cardiovascular diseases*, 2004, **47**, 116–130.
6 L. S. Goodman, *Goodman and Gilman's the Pharmacological Basis of Therapeutics*, McGraw-Hill New York, 1996.
7 K. J. McConnell, T. L. Humphries, M. A. Raebel and J. A. Merenich, *Pharmacotherapy*, 2003, **23**, 1564–1572.
8 A. Dispas, P.-Y. Sacré, E. Ziemons and P. Hubert, *J. Pharm. Biomed. Anal.*, 2022, **221**, 115071.
9 C. A. Beasley, J. Shaw, Z. Zhao and R. A. Reed, *J. Pharmaceut. Biomed. Anal.*, 2005, **37**, 559–567.
10 N. Sultana, S. Naveed and M. Arayne, *J. Chromatogr. Sep. Tech.*, 2013, **4**, 1–5.
11 V. B. Raju and A. L. Rao, *J. Chem.*, 2012, **9**, 340–344.
12 J. V. Shah, P. A. Shah, P. V. Shah, M. Sanyal and P. S. Shrivastav, *J. Pharm. Anal.*, 2017, **7**, 163–169.
13 F. Qin, D. Wang, S. Yang, L. Jing, Z. Xiong and F. Li, *Biomed. Chromatogr.*, 2012, **26**, 691–696.
14 B. Coldibeli and E. R. Sartori, *Diamond Relat. Mater.*, 2024, **142**, 110787.
15 A. A. El-Emam, S. H. Hansen, M. A. Moustafa, S. M. El-Ashry and D. T. El-Sherbiny, *J. Pharm. Biomed. Anal.*, 2004, **34**, 35–44.
16 F. F. Mohammed, K. M. Badr El-Din and S. M. Derayea, *RSC Adv.*, 2018, **8**, 16269–16277.

17 B. Acharya, A. Behera, S. Behera and S. Moharana, *Inorg. Chem. Commun.*, 2024, 112492.
18 X. Xu, R. Ray, Y. Gu, H. J. Ploehn, L. Gearheart, K. Raker and W. A. Scrivens, *J. Am. Chem. Soc.*, 2004, **126**, 12736–12737.
19 N. A. Pechnikova, K. Domvri, K. Porpodis, M. S. Istomina, A. V. Iaremenko and A. V. Yaremenko, *Aggregate*, 2025, **6**, e707.
20 S. Yang, J. Sun, X. Li, W. Zhou, Z. Wang, P. He, G. Ding, X. Xie, Z. Kang and M. Jiang, *J. Mater. Chem. A*, 2014, **2**, 8660–8667.
21 H. Li, X. He, Z. Kang, H. Huang, Y. Liu, J. Liu, S. Lian, C. H. A. Tsang, X. Yang and S. T. Lee, *Angew. Chem., Int. Ed.*, 2010, **49**, 4430–4434.
22 C. Wang, Q. Sun, C. Li, D. Tang, H. Shi, E. Liu, P. Guo, W. Xue and J. Fan, *Mater. Res. Bull.*, 2022, **155**, 111970.
23 H. L. Tran, W. Darmanto and R.-A. Doong, *Nanomaterials*, 2020, **10**, 1883.
24 Y. Liu, W. Li, P. Wu, C. Ma, X. Wu, M. Xu, S. Luo, Z. Xu and S. Liu, *Sens. Actuators, B*, 2019, **281**, 34–43.
25 M. A. Mousa, H. H. Abdelrahman, M. A. Fahmy, D. G. Ebrahim and A. H. E. Moustafa, *Sci. Rep.*, 2023, **13**, 12863.
26 M. J. Molaei, *Anal. Methods*, 2020, **12**, 1266–1287.
27 H. Kumar, J. Duhan and S. Obrai, *J. Fluoresc.*, 2025, **35**, 4321–4333.
28 P. Chen, S. Yang, F. Liu, Y. Jiang, Y. Wang, Y. Huang, J. Hu and L. Chen, *Adv. Photonics Res.*, 2023, **4**, 2200344.
29 J. Ren, L. Malfatti, S. Enzo, C. M. Carbonaro, L. Calvillo, G. Granozzi and P. Innocenzi, *J. Colloid Interface Sci.*, 2020, **560**, 398–406.
30 H. Liu, X. Zhong, Q. Pan, Y. Zhang, W. Deng, G. Zou, H. Hou and X. Ji, *Coord. Chem. Rev.*, 2024, **498**, 215468.
31 J. R. Lakowicz, *Principles of Fluorescence Spectroscopy*, Springer, 2006.
32 *ICH Guidelines: Validation of analytical procedures Q2 (R2)*, Geneva, Switzerland, 2022.
33 F. Pena-Pereira, W. Wojnowski and M. Tobiszewski, *Anal. Chem.*, 2020, **92**, 10076–10082.
34 F. R. Mansour, J. Płotka-Wasylka and M. Locatelli, *Analytica*, 2024, **5**, 451–457.
35 N. Manousi, W. Wojnowski, J. Płotka-Wasylka and V. Samanidou, *Green Chem.*, 2023, **25**, 7598–7604.
36 F. R. Mansour, A. Bedair and M. Locatelli, *Adv. Sample Prep.*, 2025, **14**, 100164.